Electrical Power and Energy Systems 177 (2026) 111827

Contents lists available at ScienceDirect

International Journal of Electrical Power and Energy Systems

journal homepage: www.elsevier.com/locate/ijepes

Avoiding flawed transmission system stability assessments with improved equivalent models of active distribution networks

Jakob Ungerland [a,*], Wolfgang Biener [a,b], Christian Schöll [c]

[a] Smart Grids, Fraunhofer Institute for Solar Energy Systems ISE, Freiburg, 79110, Germany
[b] Department of Sustainable Systems Engineering, University of Freiburg, Freiburg, 79098, Germany
[c] Asset Management, TransnetBW GmbH, Stuttgart, 70173, Germany

ARTICLE INFO

Keywords:
Stability assessment
Equivalent dynamic model
Distribution network equivalent
Distributed generation
Gray-box approach
Grid-forming converter

ABSTRACT

Stability assessments are crucial in transitioning towards a reliable renewable power system. An early identification of potential challenges allows transmission system planners to implement sustainable and cost-effective measures, ensuring stable grid operations. In this context, modeling the interaction of converter-based generation in active distribution networks with the transmission network is vital. Complexity-reduced equivalents of distribution network models facilitate comprehensive stability studies by reducing the computational load to a feasible level. This work introduces a novel method for creating equivalent distribution network models that is based on aggregating generators and loads of the detailed network model. Impedances connect the resulting aggregated components, forming the equivalent network model. This method is validated across various scenarios of grid-forming converter penetration and grid strength, and is compared with three established methods. The findings reveal that models aggregated with the industry standard method exhibit significant deviations from the detailed models and often fail to identify instabilities. Furthermore, the drawbacks of each established method are identified. In contrast, the proposed method successfully creates equivalent models that do not exceed any validation threshold values. Therefore, this work highlights the importance of employing appropriate methods for creating equivalent distribution networks to avoid erroneous assessments of system stability.

1. Introduction

1.1. Motivation

With converter-based generation emerging as the primary power source in future electricity systems, network models for stability studies must focus on both transmission and distribution networks. Understanding how converter-based generation in ADNs influences transmission system stability is crucial. However, detailed ADN representations in stability analyses require significant computational resources. To tackle this challenge, complex ADN models can be replaced with complexity-reduced EDAMs, thus facilitating comprehensive system stability studies.

The EDAM must accurately reflect the dynamic behavior of the corresponding detailed ADN. If it misses key dynamics, particularly those of converter-based generation, stability assessments will be compromised. Incorrect stability evaluations can negatively affect network planning, leading to unnecessary costs. Commercial power system simulation tools offer only insufficient support to create EDAMs for systems dominated by converter-based generation. This work assesses established and novel methods to derive EDAMs for various network conditions. The ADN models considered differ in grid strength and the ratio of grid-following converters (GFLCs) to GFMCs. The primary focus is to create EDAMs from ADNs featuring a 100 % share of converter-based generation.

1.2. Literature review

Several methods exist for deriving EDAMs. Table 1 provides a method comparison, which will be discussed in the following paragraphs. According to [1], the methods can be distinguished between approaches for networks with only conventional generation and those that incorporate both conventional and converter-based generation. The former, such as modal-based [2] and coherency-based approaches, are well established and widely available in power system simulation software.

* Corresponding author.
E-mail address: jakob.ungerland@ise.fraunhofer.de (J. Ungerland).

https://doi.org/10.1016/j.ijepes.2026.111827
Received 7 November 2025; Received in revised form 21 January 2026; Accepted 1 April 2026
Available online 16 April 2026

Table 1
Comparison of methods to derive dynamic network equivalents.

Method	Converter-Based Generation?	Detailed Network Model Necessary?	Computational Effort	References
Modal-Based	No	Yes	Low	[2]
Coherency-Based (e.g., REI)	No	Yes	Low	[3]
Parameter Identification				
– Black-Box	Yes	No	High	[4,5]
– Gray-Box Generic Model-Based	Yes	No	High	[6–9]
– Gray-Box Clustering-Based (e.g.,TCA,STCA,GCA)	Yes	Yes	Low	[1,10]

The most commonly used coherency-based approach is the REI method, developed by [3], which serves as the industry standard. The REI method generates multiple equivalent generator and load buses based on load flow results and coherency criteria, with equivalent impedances connecting these buses to an EDAM. An exemplary REI-based EDAM can be seen in Fig. 1 (b).

In contrast to modal and coherency-based methods, parameter identification techniques better suit networks with both conventional and converter-based generation [11]. These methods utilize data from simulation results or grid measurements to optimize EDAM parameters. The EDAM model structure can be either a black-box or a gray-box. Black-box models require extensive input data for training artificial neural networks [4,5]. Methods for creating gray-box models can be further categorized into approaches based on either generic models or clustering. The former methods tune parameters of generic network models to align with the corresponding detailed ADN. Typical components of these models include static and dynamic load models, as evaluated in [12,13] (e.g., constant impedance loads, constant current loads, constant power loads, induction motors), and potentially converter-based generators, as published in [6–9].

Black-box and generic EDAM derivation methods do not require insight into the detailed network model. However, they depend on extensive parameter identification data. For stability studies, the EDAM must reproduce large disturbances, so parameterization data must include such events. Moreover, calibrating black-box or generic models is computationally intensive, limiting the evaluation of many grid development scenarios.

When detailed network information is available – as in stability studies of future power systems using assumption-based ADN models – clustering-based gray-box approaches can exploit this knowledge. These methods aggregate generators and loads into clusters according to defined criteria and connect the resulting equivalent components to form the EDAM. They do not require high computational resources but rely on a thorough understanding of the network, including models of its dynamic generator and load components.

The work in [14,15] provides an overview of clustering-based methods. A common practice among transmission system operators is to aggregate all generators and loads into a single equivalent load (Netting Approach), as introduced by [16]. However, this approach neglects the distinct dynamic behaviors of individual generators and loads. The TCA [10] and the STCA [1] are developed specifically for converter-dominated systems [1,11]. Fig. 1 (c) and (d) show schematics of TCA- and STCA-based equivalent models.

The TCA clusters the detailed network's generators and loads by technology, control strategy, and voltage level [10]. Each cluster's elements are aggregated into a single equivalent component. The resulting equivalent components are connected to a busbar linked to a transformer via an equivalent impedance. This transformer connects the EDAM to a boundary bus, serving as a common link between the ADN and the transmission system. The equivalent impedance is parameterized to ensure that the steady-state power flow at the EDAM's boundary bus aligns with the one observed at the detailed ADN model's boundary bus.

However, since all equivalent components in a TCA-based EDAM are connected to one busbar, the detailed model's network topology and the individual voltage sensitivities at each point of common coupling (PCC) of the generators and loads, which we consider as a measure of grid strength, are not captured. This oversight is particularly significant for GFMCs, whose dynamic response highly depends on both factors [17].

The STCA, introduced in [1], addresses this gap in the GFMC aggregation process. It clusters GFMCs based on the detailed network's topology and voltage sensitivities ($\frac{\partial V_i}{\partial P_i}$, $\frac{\partial V_i}{\partial Q_i}$, $\frac{\partial \vartheta_i}{\partial P_i}$, and $\frac{\partial \vartheta_i}{\partial Q_i}$) at the PCC i, where P and Q represent active and reactive power, respectively, and V and ϑ denote voltage phasor magnitude and angle. The aggregated equivalent GFMCs are connected through equivalent impedances in the EDAM, matching the detailed network's topology and voltage sensitivities at the corresponding PCCs [1,18]. An additional slack load component is parameterized to ensure that the steady-state power flow at the EDAM's boundary bus aligns with the one at the detailed ADN model's boundary bus. When parameterized as a negative load, this slack component behaves as a static generator.

Both [1,18] leave a crucial research gap unaddressed, as they validated the TCA and STCA for networks with a substantial GFMC share, specifically 60 % GFMCs and 40 % GFLCs of the total converter-based generation. Research has not yet explored networks with varying GFMC to GFLC ratios or examined how different transmission grid strengths, measured at the boundary bus, affect EDAM performance. Especially when the GFMC share is low and the ADN is weak, the dynamic responses of GFLCs and dynamic loads have a greater influence on the ADN's behavior, which previous methods do not capture. Additionally, there is no thorough analysis of the industry standard REI method applied on networks with GFMCs. Evaluating EDAM derivation methods for varying grid states is crucial, as they are integral to power system stability studies.

1.3. Contribution and paper organization

This paper targets large-signal stability studies of future power systems using assumption-based ADN models. Motivated by this scope, we adopt clustering-based gray-box EDAM derivation methods that exploit detailed network information and, specifically, introduce the GCA for constructing EDAMs in converter-dominated systems. To address the gap identified in Section 1.2, we evaluate GCA alongside three established methods (REI, TCA, and STCA) on an ADN model across grid states that vary in GFMC to GFLC ratios and boundary bus grid strength. In all scenarios, converter-based generation supplies 100 % of the ADN's demand. For each scenario, we derive EDAMs with all four methods and perform phasor-domain root mean square (RMS) simulations for five events in the transmission system (frequency ramps, a voltage angle step, and a short circuit). We then compare each EDAM's dynamic response with the corresponding detailed ADN model and assess whether it reproduces the detailed model's stability or instability.

The main contributions of this paper are as follows:

1. We propose the GCA to capture the dynamic behavior of detailed ADN models by clustering GFMCs, GFLCs, and dynamic loads according to voltage sensitivities and the detailed network's topology.
2. We quantify deviations in the dynamic behavior between detailed ADN models and their corresponding EDAMs derived by REI, TCA, STCA, and GCA.
3. We conduct a sensitivity analysis of the REI-, TCA-, STCA-, and GCA-based EDAM across scenarios differing in GFMC to GFLC ratios and grid strengths at the boundary bus.

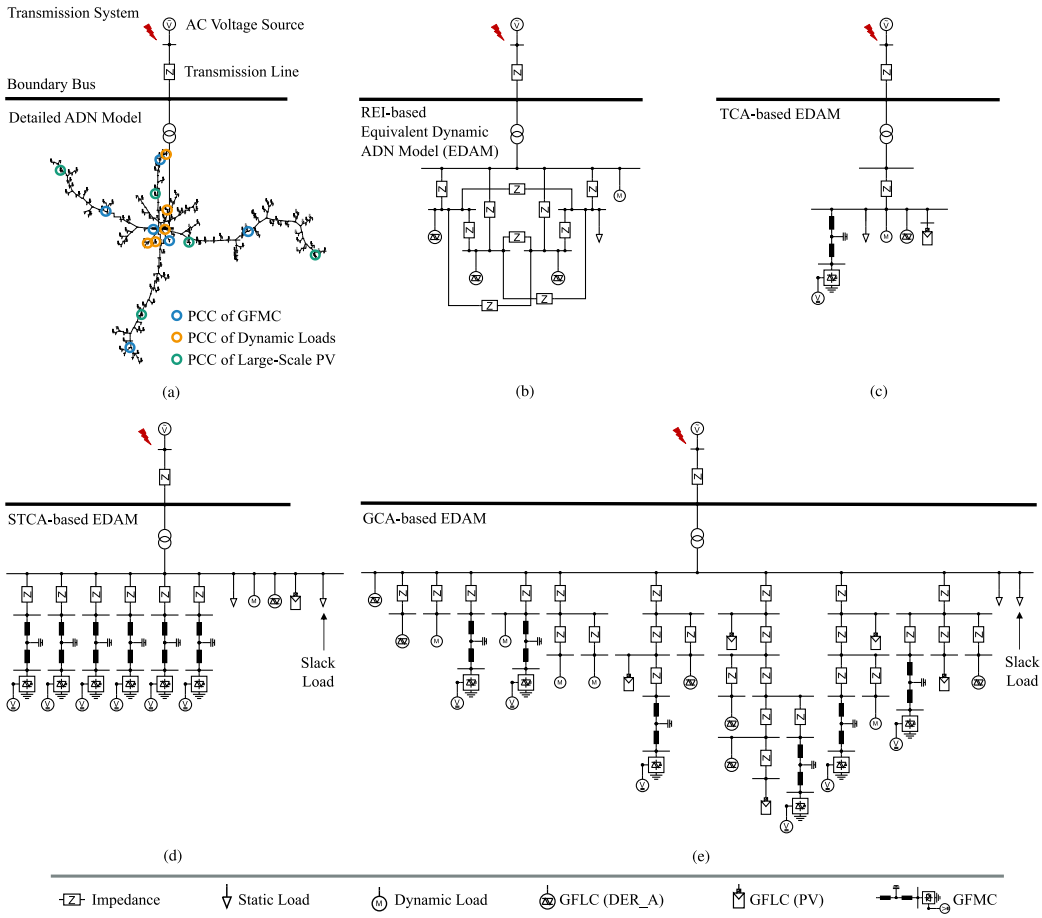

Fig. 1. Schematic of detailed ADN model (a) and equivalent dynamic ADN model (EDAM) derived by REI (b), TCA (c), STCA (d), and GCA (e)

4. We demonstrate that industry standard REI method for EDAM creation is not suitable for stability assessment of future ADNs.

Section 2 describes the scenarios and both detailed and equivalent ADN models utilized for the evaluation of the EDAM derivation methods in this work. Simulations results as well as evaluation metrics are provided in Section 3. The results and limitations are discussed in Section 4 and this work concludes in Section 5 with a summary.

2. Active distribution network models

2.1. Scenario overview

To thoroughly assess each EDAM derivation method under variable grid conditions, multiple scenarios are simulated. These scenarios vary based on the GFMC/GFLC ratio within the ADN and the ADN's grid strength, i.e., the SCR at the lower voltage side of the high voltage (HV)/medium voltage (MV) transformer. In all scenarios, the ADN is supplied entirely by converter-based generation.

We span 0 % to 60 % GFMC penetration within the ADN, reflecting a gradual increase in plants with grid-forming properties. Higher shares are omitted as they appear neither economically justified nor technically necessary for ADNs. Lower penetrations are included because the minimum GFMC share for stable operation is system-dependent and unresolved. They are also essential for simulating transitional stages towards higher GFMC penetration. Low local GFMC shares (0 % to 20 %) may arise when neighboring ADNs provide sufficient grid-forming properties. According to [19,20], stable operation near 100 % converter-based generation penetration may require a 10 % to 35 % GFMC share in Great Britain and 30 % to 40 % in Ireland. Beyond these indicative values, [20] notes that the minimum share remains an open question and emphasizes its dependence on system characteristics, including the spatial distribution of generation.

Table 2 provides an overview of the considered scenarios and their respective scenario names. An SCR of 1.5 is considered as a weak, an SCR of 5 as a modest, and an SCR of 10 as a strong connection to the transmission grid [21,22]. The GFMC shares range from 0 %, implying that the ADN's demand is met by GFLCs, to 60 %, representing a significant GFMC penetration scenario.

The SCR of a converter is calculated according to [16] as

$$\mathrm{SCR} = \frac{S_{\mathrm{SC}}}{S_{\mathrm{N}}}, \tag{1}$$

where S_{N} is the rated apparent power of the converter and S_{SC} the short circuit apparent power of the AC system as defined as

$$S_{\mathrm{SC}} = \frac{V_{\mathrm{AC}}^2}{Z_{\mathrm{th}}}, \tag{2}$$

where V_{AC} is the converter voltage and Z_{th} the Thévenin equivalent impedance [23] of the AC system. To define the SCR of an ADN, S_{N} is the summed up apparent power of each generator within the ADN. S_{SC} is the apparent short circuit power at the lower voltage side of the HV/MV transformer. Z_{th} is defined as the downstream impedance associated with the ADN. As S_{N} remains constant for all scenarios, the internal impedance of the AC voltage source in the transmission system is adapted to fit the required S_{SC}.

For all network scenarios of Table 2, the following events are simulated:

Table 2
Overview of scenario names.

	GFMC share			
	0 %	20 %	40 %	60 %
SCR = 1.5	0/100-1.5	20/80-1.5	40/60-1.5	60/40-1.5
SCR = 5	0/100-5	20/80-5	40/60-5	60/40-5
SCR = 10	0/100-10	20/80-10	40/60-10	60/40-10

Table 3
Generation and demand of the network model of scenario *60/40-1.5* with a 60 % GFMC share and an SCR of 1.5.

	Voltage Level	Type	Actual Power	Number of Units
Generation	220 kV	Voltage Source	0.4 MW (Slack)	1
	10 kV	GFLC		
		– PV	0.9 MW	5
		– DER_A	15.3 MW	91
		GFMC	23.8 MW	6
Demand	10 kV	Dynamic Composite Load		
		– Three-Phase Motor	16.1 MW	15
		– One-Phase Motor	7.9 MW	5
		– Electronic Load	6.5 MW	5
		– Static Load	2.6 MW	5
		Constant Impedance	6.9 MW	117

- Frequency ramps with a Rate of Change of Frequency (RoCoF) of 0.5 Hz/s, adjusting from 50 Hz to targeted frequencies of 48.5 Hz, 50.25 Hz, and 51.5 Hz.
- Voltage angle jump from 0° to 23°.
- Three-phase short circuit lasting 130 ms.

2.2. Detailed ADN Model

The focus of this research is the stability of decentralized converter-based systems. Hence, the demand of the ADN models utilized in this work is met entirely by converter-based generation. Table 3 provides the generation and demand details of the ADN in the *60/40-1.5* scenario, where 60 % of the ADN's demand is met by GFMCs, and the remaining 40 % is generated by GFLCs. This scenario describes a weak grid with an SCR of 1.5.

GFLCs are modeled as large-scale photovoltaic power plants (PVs) as described in [24] and as generic distributed energy resources using the DER_A model introduced in [25]. GFMCs are represented as droop-controlled converters based on the template provided by *DIgSILENT* [26]. The GFMC's output current is limited to 1 pu. On the DC side, the GFMC is connected to a battery energy storage system.

The ADN's demand, which is consistent across all scenarios, is modeled with both dynamic (around 83 % of total demand) and constant impedance loads (around 17 % of total demand). For the former, the composite load model introduced in [27] is used, comprising three three-phase motors, an one-phase motor, an electric load, and a static load.

Fig. 1 (a) depicts the transmission network and the ADN. The former is modeled as a 220 kV AC voltage source with an internal impedance and a 100 km transmission line. The line is modeled according to the subtransmission line of the CIGRE benchmark system in the European configuration [28]. The open-ring ADN structure and the demand distribution are based on a 10 kV network from the open-source tool DINGO [29]. The PCCs of GFMCs, large-scale PVs, and dynamic loads are marked in Fig. 1 (a) to illustrate the distribution within the ADN.

2.3. Equivalent Dynamic ADN Models

2.3.1. REI-based Model

REI, widely implemented in commercial power system simulation tools like *DIgSILENT PowerFactory*, sets the industry standard. As noted in Section 1.2, transmission system operators often aggregate an ADN to one equivalent load for system stability studies. However, REI, by distinguishing between generation and demand, offers superior precision. By connecting the equivalent components via impedances, it more accurately approximates the relationship between generation and demand within the detailed network.

The REI method aggregates loads and generators of the detailed network model to equivalent components based on coherency criteria (similar rotor angle swings). It generates multiple aggregated equivalent components connected via impedances to retain the electrical distances from loads and generators to the boundary bus (Fig. 1 (b)). As the coherency-based aggregation relies on synchronous generation, converter-based generators are aggregated as static components neglecting their dynamic responses. A detailed description of the method can be found in [3].

2.3.2. TCA-based Model

The TCA as a clustering-based approach clusters all generators and loads of the detailed network and aggregates them to an equivalent component per cluster. As mentioned, the detailed ADN model comprises three different converter control strategies: GFMC and two different GFLCs (large-scale PV and DER_A model). Also, two different load models are used: dynamic composite load and constant impedance load. This leads to five clusters, i.e., five equivalent components, for the TCA-based EDAM (Fig. 1 (c)). The active and reactive power generation and demand of the equivalent components is calculated by summing up the active and reactive power generation and demand of all individual generators and loads per cluster in the detailed network.

All equivalent components are connected to the lower voltage side of the transformer by an impedance. This impedance is parameterized to match the steady-state power flow at the EDAM's boundary bus to the one at the detailed ADN model's boundary bus. [10] describes the TCA in more detail. Note that all GFMCs in the studied ADN have the same control strategy, which is droop-based control. If there were different GFMC control strategies in the network being aggregated, it would lead to a respective increase in the number of clusters, i.e., more equivalent GFMC components.

2.3.3. STCA-based Model

The equivalent GFLCs and load components found in the TCA-based EDAM are also present in the EDAM derived by the STCA shown in Fig. 1 (d). However, the STCA further integrates the grid's strength and the network topology in the GFMC aggregation process since both factors are essential to capture the dynamics of GFMCs properly. Since all GFMCs within the detailed network are located in different branches, a GFMC aggregation that preserves relevant dynamics of the network is not feasible. As a solution, the six GFMCs are considered individually and connected in parallel within the EDAM.

The equivalent impedances connecting the equivalent GFMCs with the lower voltage side of the transformer are parameterized to represent the grid's strength at the PCCs of the corresponding GFMCs in the detailed network. As introduced in [1], the voltage sensitivities $\frac{\partial V_i}{\partial P_i}$, $\frac{\partial V_i}{\partial Q_i}$, $\frac{\partial \vartheta_i}{\partial P_i}$, and $\frac{\partial \vartheta_i}{\partial Q_i}$ are a suitable measure to consider the grid strength at the GFMC's PCC i. Hence, optimal parameters of the equivalent impedances minimize the differences in voltage sensitivities at GFMC's PCC in the detailed network compared to those in the EDAM. With this impedance parameterization, the steady-state power flow at the EDAM's boundary bus is unlikely to match that of the detailed network's boundary bus. Thus, an additional static load (slack load) is introduced to align the power flows. More detailed information about the STCA can be found in [1,18].

2.3.4. GCA-based Model

As mentioned in Section 1.2, previous work validated the STCA in networks with a high GFMC share. However, with low GFMC shares and weak grid conditions, the GFLCs and dynamic loads play an increasingly crucial role in the ADN's dynamic response to events. In such cases, these components must be represented more distinctly in the EDAM to better reproduce the detailed ADN's dynamic behavior. Therefore, we propose a more general approach with the GCA.

Here, we consider the voltage sensitivities at the PCCs of generators and loads, and the network topology not only in the aggregation process of the GFMCs, but also of the GFLCs and dynamic loads. The resulting EDAM is shown in Fig. 1 (e). In this model, GFMCs, large-scale PVs, and dynamic loads of the detailed network are not aggregated to a fewer number of equivalent components due to their spatial distribution within the detailed network and the low complexity reduction achieved by an aggregation. The remaining 91 GFLCs are aggregated to six equivalent GFLCs, where only neighboring GFLCs are reduced to one equivalent component to approximate the detailed network's behavior.

The equivalent impedances of this GCA-based EDAM are parameterized to match the voltage sensitivities at the PCCs of components to the ones at the corresponding PCCs in the detailed network. When aggregating multiple components, the equivalent impedance is parameterized such that the voltage sensitivities at the equivalent component's PCC represent the respective voltage sensitivities in the detailed ADN model.

2.3.5. Derivation of voltage sensitivities

Both STCA and GCA depend on the calculation of voltage sensitivities $\frac{\partial V_i}{\partial P_i}$, $\frac{\partial V_i}{\partial Q_i}$, $\frac{\partial \vartheta_i}{\partial P_i}$, and $\frac{\partial \vartheta_i}{\partial Q_i}$. A voltage sensitivity at a bus quantifies how its voltage magnitude or angle changes in response to variations in the active or reactive power injected at that bus. As established in our previous work [1], the inverse Jacobian matrix used in the Newton–Raphson power flow serves as a sensitivity matrix from which these quantities can be derived.

Around a steady-state operating point with bus 1 as slack node, a first-order linearization yields

$$\begin{bmatrix} \Delta P_2 \\ \vdots \\ \Delta P_n \\ \Delta Q_2 \\ \vdots \\ \Delta Q_n \end{bmatrix} = \begin{bmatrix} \frac{\partial P_2}{\partial \vartheta_2} & \cdots & \frac{\partial P_2}{\partial \vartheta_n} & \frac{\partial P_2}{\partial V_2} & \cdots & \frac{\partial P_2}{\partial V_n} \\ \vdots & \ddots & \vdots & \vdots & \ddots & \vdots \\ \frac{\partial P_n}{\partial \vartheta_2} & \cdots & \frac{\partial P_n}{\partial \vartheta_n} & \frac{\partial P_n}{\partial V_2} & \cdots & \frac{\partial P_n}{\partial V_n} \\ \frac{\partial Q_2}{\partial \vartheta_2} & \cdots & \frac{\partial Q_2}{\partial \vartheta_n} & \frac{\partial Q_2}{\partial V_2} & \cdots & \frac{\partial Q_2}{\partial V_n} \\ \vdots & \ddots & \vdots & \vdots & \ddots & \vdots \\ \frac{\partial Q_n}{\partial \vartheta_2} & \cdots & \frac{\partial Q_n}{\partial \vartheta_n} & \frac{\partial Q_n}{\partial V_2} & \cdots & \frac{\partial Q_n}{\partial V_n} \end{bmatrix} \begin{bmatrix} \Delta \vartheta_2 \\ \vdots \\ \Delta \vartheta_n \\ \Delta V_2 \\ \vdots \\ \Delta V_n \end{bmatrix}, \tag{3}$$

which we write compactly as

$$\Delta \mathbf{Z} = \mathbf{G}\, \Delta \mathbf{X}, \tag{4}$$

$$\Delta \mathbf{X} = \mathbf{G}^{-1} \Delta \mathbf{Z} = \mathbf{F}\, \Delta \mathbf{Z}, \tag{5}$$

with

$$\mathbf{F} = \begin{bmatrix} \mathbf{H} & \mathbf{N} \\ \mathbf{J} & \mathbf{L} \end{bmatrix} \tag{6}$$

as the inverse Jacobian matrix.

We focus on the diagonal entries of **H**, **N**, **J**, and **L**, which capture the local response of each bus to its own power changes. These entries correspond to the sensitivities $\frac{\partial V_i}{\partial P_i}$, $\frac{\partial V_i}{\partial Q_i}$, $\frac{\partial \vartheta_i}{\partial P_i}$, and $\frac{\partial \vartheta_i}{\partial Q_i}$. It becomes evident that voltage sensitivities can be obtained from a simple load flow calculation, making STCA as well as GCA fast and straightforward to apply.

2.3.6. Equivalent impedances parameterization

The parameterization of the equivalent impedances in the TCA, STCA, and GCA aims to minimize the mismatch in voltage sensitivities between the detailed and the equivalent network model at relevant nodes (PCCs of GFMCs, GFLCs, dynamic loads, and branch nodes with three or more connections). Since an exact match is hardly attainable, an error tolerance of $\epsilon = \pm 5\%$ has been found sufficient for rapid parameterization of a well-performing EDAM [1,18,30].

In the EDAM, the voltage sensitivities of a node depend on the equivalent impedance's real and imaginary parts, R and X. Accordingly, the optimization problem can be written as introduced in [30], that is,

$$\underset{R \in \mathbb{R}^n,\, X \in \mathbb{R}^n}{\text{minimize}} \quad \sum_{i=1}^{n} \sum_{j=1}^{4} (y_{ji}^{\text{det}}(R, X) - y_{ji}^{\text{eq}}(R, X))^2 \tag{7a}$$

$$\text{subject to} \quad 0 \le R_i \le R_{\max} \quad \forall i = 1, 2, \ldots, n, \tag{7b}$$

$$0 \le X_i \le X_{\max} \quad \forall i = 1, 2, \ldots, n. \tag{7c}$$

The function $y(R, X)$ returns the voltage sensitivities for each relevant node i,

$$\begin{pmatrix} y_{1i}(R, X) \\ y_{2i}(R, X) \\ y_{3i}(R, X) \\ y_{4i}(R, X) \end{pmatrix} := \begin{pmatrix} \frac{\partial V_i}{\partial P_i}(R, X) \\ \frac{\partial V_i}{\partial Q_i}(R, X) \\ \frac{\partial \vartheta_i}{\partial P_i}(R, X) \\ \frac{\partial \vartheta_i}{\partial Q_i}(R, X) \end{pmatrix}. \tag{8}$$

Here, $y^{\text{det}}(R, X)$ gives sensitivities of the detailed model and $y^{\text{eq}}(R, X)$ those of the EDAM. The bounds $R_{\max}$ and $X_{\max}$ depend on the network and PCCs of GFMCs, GFLCs, and dynamic loads.

If each GFMC, GFLC, and dynamic load is modeled individually in the EDAM, $y^{\text{det}}(R, X)$ and $y^{\text{eq}}(R, X)$ both lie in $\mathbb{R}^{4 \times n}$, where n is the number of equivalent impedances. With aggregation, n counts only GFMCs, GFLCs, and dynamic loads kept individual. Impedances for the remaining aggregated equivalent components are tuned so that PCC voltage sensitivities lie within the range spanned by the sensitivities of all GFMCs, GFLCs, and dynamic loads in the corresponding cluster of the detailed network model [30].

3. Simulation results

3.1. Setup and validation methodology

This study involves simulating five distinct events, comparing the responses from a detailed ADN model against those from corresponding EDAMs derived using REI, TCA, STCA, or GCA for each scenario outlined in Table 2. RMS simulations were performed in *DIgSILENT PowerFactory* with an integration time step of 1 ms. The five events listed in Section 2.1, which are initiated either by the voltage source or at the PCCs for short circuit faults, occur at 0 s.

The goal is to validate whether EDAMs can accurately reproduce the dynamic behavior of the detailed ADN model, particularly at the boundary bus. To this end, deviations in active and reactive power flows at the boundary bus are calculated at each simulation time step. Three error metrics, namely mean absolute error (MAE), mean error (ME), and root mean square error (RMSE), are used to quantify these deviations:

- mean absolute error MAE:

$$\delta_{\text{MAE}} = \frac{\sum_{n=1}^{N} |x_{\text{E}}(n)|}{N} \tag{9}$$

- mean error ME:

$$\delta_{\text{ME}} = \frac{\sum_{n=1}^{N} x_{\text{E}}(n)}{N} \tag{10}$$

- root mean square error RMSE:

$$\delta_{\text{RMSE}} = \sqrt{\frac{\sum_{n=1}^{N} x_{\text{E}}^2(n)}{N}} \tag{11}$$

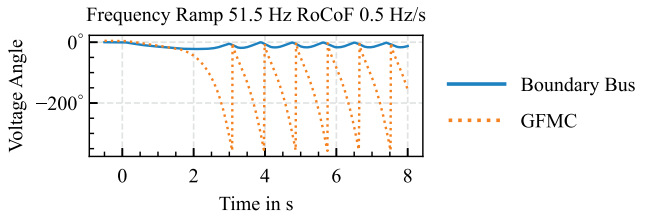

Fig. 2. *Scenario 60/40-5*: Voltage angles at the boundary bus and at a GFMC in the detailed ADN model illustrating the instability.

$x_E(n)$ denotes the active or reactive power deviation between the detailed ADN model and the EDAM at the boundary bus for each time step n, and N represents the total number of time steps. Given the EDAMs are parameterized based on the steady-state power flow (Section 2), deviations prior to the event are considered negligible. The relevant time frame for calculating these error metrics extends from 0 s to 5 s after the event initiation.

$x_E(n)$ is defined as $p_E(n)$ for active power, that is,

$$p_E(n) = \frac{P_{ADN}(n) - P_{EDAM}(n)}{P_0}, \tag{12}$$

where $P_0 = 40$ MW as the detailed ADN model's active power demand. Similar to (12), $x_E(n)$ is defined as $q_E(n)$ for reactive power with $Q_0 = 10$ Mvar as the detailed ADN model's reactive power demand.

The guidelines in [31] provide threshold values for δ_{MAE} and δ_{ME}. If the error metrics for both active and reactive power are below 0.17 for δ_{MAE} and within the range of −0.15 to 0.15 for δ_{ME}, respectively, the EDAM is considered a valid representation of the detailed ADN model. The system behavior is considered unstable if the system variables observed in the simulations are either poorly damped to such an extent that they diverge or no longer show decaying oscillations.

3.2. Exemplary case studies

3.2.1. Frequency ramp instability (Scenario 60/40-5)

An unstable detailed ADN model is illustrated exemplary with the event of a frequency ramp to 51.5 Hz with a RoCoF of 0.5 Hz/s in a network with a GFMC penetration of 60 % and an SCR of 5. This event leads to an instability in the detailed ADN model as shown in Fig. 2. Here, the voltage angles measured at the boundary bus and at one exemplary GFMC of the detailed ADN model are compared. It becomes clear that both voltage angles deviate significantly leading to an unstable model.

The dynamic behavior of the EDAMs compared to the detailed ADN model are exemplified for the same event in Fig. 3, where active and reactive power flows from the transmission to the distribution networks are analyzed. Notably, significant oscillations are observed in the detailed ADN model, the TCA-based EDAM, the STCA-based EDAM, and the GCA-based EDAM. In contrast, the REI-based EDAM does not capture these oscillations, exhibiting stable behavior instead.

3.2.2. Short circuit in weak grid (Scenario 0/100-1.5)

As an additional example, Fig. 4 shows the active and reactive power flows at the boundary bus of the detailed and equivalent ADN models. The GFMC penetration is 0 % and the ADN model is connected to a weak transmission system, i.e., a SCR of 1.5 at the boundary bus. The simulated event is a short circuit with a duration of 130 ms.

The REI-based EDAM reaches steady-state values without significant dynamics and, hence, does not capture the dynamic behavior of the detailed ADN model. This is expected as the equivalent converters are modeled as static components without dynamic responses (Section 2.3.1). Since no GFMCs are present, the EDAMs derived by TCA and STCA have a similar behavior, which differs significantly from the one of the detailed ADN model. All GFLCs are aggregated into a single

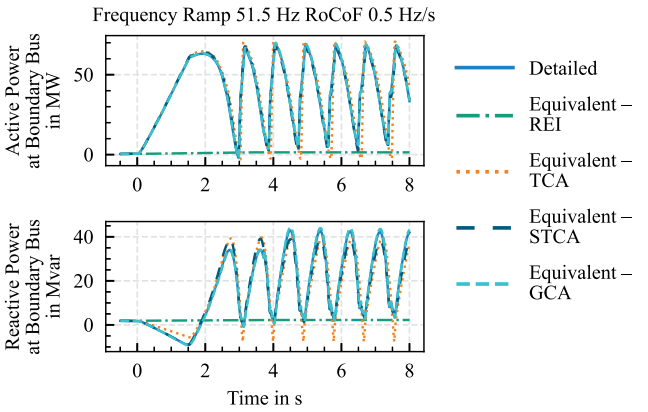

Fig. 3. *Scenario 60/40-5*: Active and reactive power flow from the transmission system to the detailed and equivalent ADN models measured at the boundary bus; positive reactive power values: over-excited state; negative reactive power values: under-excited state.

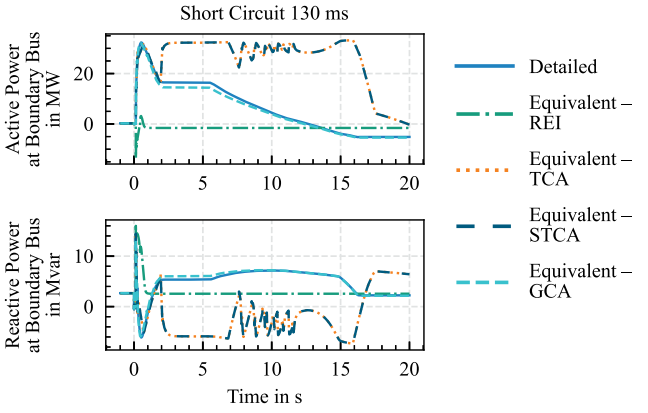

Fig. 4. *Scenario 0/100-1.5*: Active and reactive power flow from the transmission system to the detailed and equivalent ADN models measured at the boundary bus; positive reactive power values: over-excited state; negative reactive power values: under-excited state.

equivalent component in both the TCA- and STCA-based EDAMs, and connected to the transformer's lower voltage side (Section 2.3.2 and Section 2.3.3). Consequently, the equivalent GFLC's reactive power is controlled based on the voltage measured at that single busbar. Because the equivalent GFLC supplies large reactive currents, its current limits are exceeded repeatedly in the post-fault period, causing oscillations visible in Fig. 4 between approximately 7 s and 12 s.

The EDAM derived by GCA distinguishes between the individual GFLCs of the detailed ADN model (Section 2.3.4). By incorporating voltage sensitivities and network topology into the aggregation process, the voltages measured at the equivalent GFLC's PCC and, therefore, the reactive currents, more closely match those of the detailed ADN model. As the GCA-based EDAM only supplies realistic reactive currents, which do not exceed limits, it reproduces the power flows of the detailed ADN model correctly.

3.3. Cross-scenario validation

A more comprehensive analysis is given in Fig. 5. Here, the share of failed error metrics δ_{MAE} and δ_{ME}, i.e., the error metrics exceed threshold values defined in [31], for both active and reactive power is shown. This heatmap is divided into five different events, four EDAM derivation methods, four GFMC penetration scenarios, and three SCR scenarios. The less validation thresholds are exceeded the better the

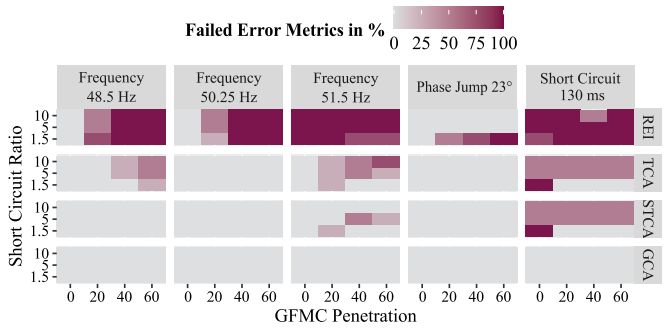

Fig. 5. Heatmap of failed error metrics δ_{MAE} and δ_{ME} for both active and reactive power of the evaluated EDAMs for different scenarios; error metrics are considered as failed if they exceed the allowed threshold as introduced in [31].

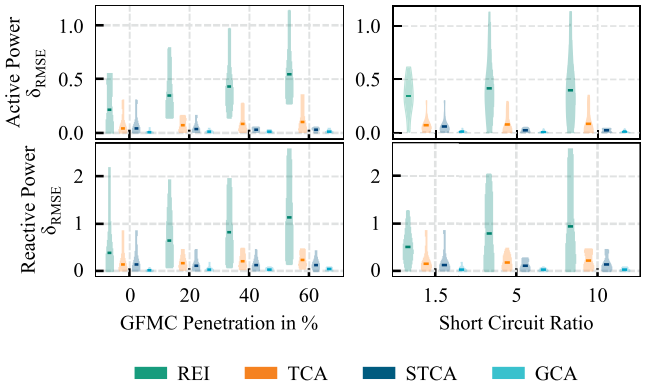

Fig. 6. Violin plots with average values of active and reactive power deviations δ_{RMSE} of different EDAMs dependent on the GFMC penetration and SCR scenarios.

EDAM reproduces the dynamic behavior of the corresponding detailed network.

The results indicate significant active and reactive power deviations of the REI-based EDAM in all GFMC penetration and grid strength scenarios. In 45 of the 60 calculated scenarios, the threshold of either δ_{MAE} or δ_{ME} is exceeded. EDAMs derived by TCA as well as STCA also deviate from the corresponding detailed ADN models for some scenarios. In total, EDAM derived by TCA exceed threshold values of δ_{MAE} or δ_{ME} in 21 of the 60 scenarios, while the STCA-based EDAM is invalid in only 12 scenarios. Both TCA- and STCA-based EDAMs capture the frequency change to 50.25 Hz and the phase jump to 23° without validation violations. Opposed to all other EDAMs, the introduced GCA-based EDAM does not exceed any threshold and, hence, reproduces the dynamic behavior of the detailed network model very well.

3.4. Sensitivity to GFMC penetration and grid strength

Fig. 6 shows the density of δ_{RMSE} deviations for both active and reactive power of the investigated EDAMs compared to their corresponding detailed network. The left side of the plots focuses on the four GFMC penetration scenarios and the right side shows the deviations dependent on the three considered SCR scenarios. Similarly to the previous deductions, REI-based EDAMs deviate significantly from the dynamic behavior of the detailed network model.

Increased GFMC penetration tends to amplify the discrepancies observed in TCA-based EDAMs, especially for active power deviations. Conversely, EDAMs derived by STCA generally better replicate the dynamic behavior of the corresponding detailed ADN models in scenarios

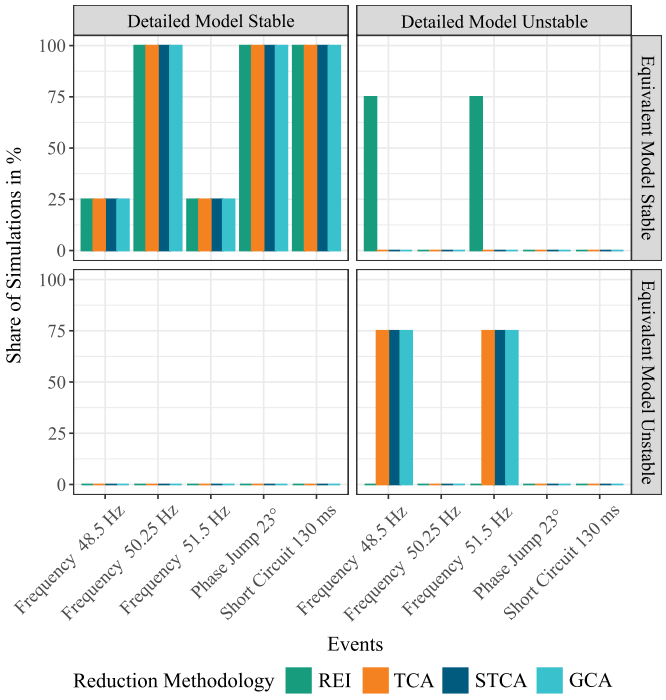

Fig. 7. Stability assessment of EDAMs derived by REI, TCA, STCA, and GCA.

with higher GFMC penetration. Weak grids, characterized by low SCR, lead to more pronounced deviations in STCA-based EDAMs compared to those observed in grids with higher SCR. It becomes clear that the introduced GCA is the only approach to create EDAMs that result in low δ_{RMSE} deviations across all GFMC penetration and SCR scenarios.

3.5. Accuracy of stability assessment

In addition to analyzing deviations, this work addresses stability assessments of EDAMs. Fig. 7 is segmented into four bar plots stating the stability of both detailed ADNs model and EDAMs for each event. Note that one event is simulated in four GFMC penetration and three SCR scenarios.

It can be seen that several events lead to an unstable detailed ADN model, specifically the frequency jump to 48.5 Hz and 51.5 Hz in 75 % of the cases, i.e., in nine GFMC penetration and SCR scenarios. EDAMs derived by TCA, STCA, and GCA capture these instabilities, while REI-based EDAMs lead to the incorrect conclusion that the detailed models are stable.

3.6. Model complexity and computational efficiency

The scenario *60/40-5* with the 130 ms short circuit fault is used to analyze the reduction in model complexity, i.e., simulation time and number of nodes. Table 4 compares the EDAMs derived by REI, TCA, STCA, and GCA. The former three methods reduce the detailed ADN model significantly from 195 nodes to two, five, and seven nodes. Such a model reduction leads to a distinct reduction in simulation time. Here, the REI-based EDAM enables the fastest simulation.

The consideration of voltage sensitivities and network topology within GFLC and dynamic load aggregation process inevitably increases model complexity. Hence, the EDAM derived by GCA is the most complex EDAM in terms of node number and simulation time. The 195 nodes are reduced to 27 nodes and the simulation is performed in around 21 % of the detailed ADN model's simulation time.

Table 4
Reduction in model complexity by EDAMs.

ADN Model Aggregation Method	Number of Nodes	Simulation Time Relative to the Detailed Model
None (Detailed Model)	195	100 %
Equivalent – REI	5	3 %
Equivalent – TCA	2	8 %
Equivalent – STCA	7	12 %
Equivalent – GCA	27	21 %

4. Discussion

As a growing share of generation is located in distribution networks, stability studies must capture ADN dynamics via equivalent EDAMs, not only transmission behavior. Clustering-based gray-box EDAMs enable rapid derivation from detailed ADN models and static load flow data, whereas black-box or generic model-based gray-box methods rely on dynamic data.

The complexity of EDAMs derived by clustering-based approaches scales with the number of clusters and ADN diversity. The proposed GCA forms clusters by generation and load technology, control strategy, network topology, and PCC voltage sensitivities. In our case, the GCA-based EDAM reduces nodes by 86 % and simulation time by 79 %. Greater reductions could be possible with generic model-based gray-box or black-box EDAMs, but clustering-based methods demand less computational effort and facilitate embedding diverse ADN variants in transmission studies to probe stability sensitivities.

To balance accuracy and simulation time in extensive simulations, adaptively switching EDAM complexity based on event and grid state is promising. For instance, TCA and STCA are sufficient for GFMC penetrations below 20 % except during short circuits. A fast mechanism to select the appropriate reduction methodology per event and network is a worthwhile future task.

While our scenarios target converter-dominated ADNs, the GCA readily accommodates additional dynamic resources such as wind plants with doubly fed induction machines or distributed synchronous generators by forming dedicated clusters per generation technology and control strategy. We expect our main findings to carry over. REI-based EDAMs may perform relatively better when synchronous machines are present, whereas voltage sensitivity- and topology-aware clustering remains advantageous as the number and diversity of distributed units increases. Evaluating cases with substantial shares of doubly fed induction machines and residual synchronous generation is left for future work.

Considering electromagnetic transients (EMT) in stability studies is increasingly relevant [32]. Because clustering-based gray-box methods retain the dynamic models of loads and generators, the GCA should require minimal adaptation when aggregating a detailed ADN developed within an EMT framework. However, careful consideration must be given to the intended purpose of the generated EMT model, as aggregation can remove essential transient detail and thereby undermine the validity of EMT based analyses. Validation metrics may also need adaptation, potentially favoring comparisons of instantaneous values over RMS quantities.

This study examined discrete GFMC penetration and SCR steps, and specific events. Intermediate scenarios, broader generator's PCC variability, varying GFLC cluster counts, rural areas with higher generation than consumption, and interactions among multiple GCA-based EDAMs through transmission should be explored in future work. Incorporating a determination of grid strength based on Equivalent Short-Circuit Ratio (ESCR) [22] could further refine the aggregation process by accounting for both grid-forming and grid-following contributions to grid strength on a node-specific basis and with regard to the network topology.

5. Conclusion

This paper evaluates the REI, TCA, and STCA methods for creating EDAMs of converter-dominated ADN models, identifying their limitations in simulating short circuit faults, as well as phase and frequency events across different GFMC penetration and SCR scenarios. EDAMs created with the industry standard REI method consistently show significant deviations in all scenarios. TCA-based EDAMs exhibit decreasing validity with increased GFMC penetration, while STCA-based EDAMs perform better under conditions of high GFMC penetration and high SCR.

Based on these observations, we propose the GCA to more accurately reflect the dynamic behavior of detailed ADN models. This enhanced aggregation process incorporates considerations of voltage sensitivities and network topology not only in the GFMC aggregation but also extends to the aggregation of dynamic loads and GFLCs. EDAMs produced using this GCA successfully replicate the dynamic behavior of their corresponding detailed ADN models without any validation violations.

Furthermore, the study examines the accuracy of stability assessments using EDAMs. The REI method leads to incorrect stability assessments in multiple scenarios. Opposed to the other methods, REI is implemented in commercial power system simulation tools and, hence, widely used in industry practices. The flawed stability assessments shown in this work highlight the importance for power system planners to utilize methods that are more suitable for converter-dominated systems to ensure accurate and reliable assessments.

CRediT authorship contribution statement

Jakob Ungerland: Writing – review & editing, Writing – original draft, Visualization, Validation, Supervision, Software, Methodology, Investigation, Funding acquisition, Formal analysis, Data curation, Conceptualization. **Wolfgang Biener:** Writing – review & editing, Visualization, Methodology, Formal analysis, Conceptualization. **Christian Schöll:** Writing – review & editing, Validation.

Declaration of competing interest

The authors declare that they have no known competing financial interests or personal relationships that could have appeared to influence the work reported in this paper.

Acknowledgments

The work presented in this paper has been supported by the German Federal Ministry for Economic Affairs and Energy (BMWE) within the scope of the research project "SUREVIVE" (FKZ 03EI6123) and by a fellowship of the German Academic Exchange Service (DAAD).

Data availability

Data will be made available on request.

References

[1] Ungerland J, Poshiya N, Biener W, Lens H. A voltage sensitivity based equivalent for active distribution networks containing grid forming converters. IEEE Trans Smart Grid 2022;14:2825–36. http://dx.doi.org/10.1109/TSG.2022.3221874.
[2] Davison EJ. A method for simplifying linear dynamic systems. IEEE Trans Autom Control 1966;11:93–101.
[3] Dimo P. Nodal analysis of power systems. Editura Academiei Republicii Socialisté România; 1975, URL https://www.osti.gov/biblio/7233051.
[4] Liu Z, Bornhorst N, Wende-von Berg S, Braun M. A grid equivalent based on artificial neural networks in power systems with high penetration of distributed generation with reactive power control. In: IEEE conference on sustainable energy supply and energy storage systems. Hamburg; 2020.

[5] Azmy AM, Erlich I, Sowa P. Artificial neural network-based dynamic equivalents for distribution systems containing active sources. IET Proc - Gener Transm Distrib 2004;151:681–8. http://dx.doi.org/10.1049/ip-gtd:20041070.
[6] Zali SM, Milanović JV. Generic model of active distribution network for large power system stability studies. IEEE Trans Power Syst 2013;28:3126–33. http://dx.doi.org/10.1109/TPWRS.2012.2233223.
[7] Wu X, Lei X, Lan Y, Monti A, Gao F. A new dynamic equivalent of active distribution network for transient analysis. In: IEEE international conference on power system technology. 2018, p. 529–36. http://dx.doi.org/10.1109/POWERCON.2018.8601748.
[8] Fulgêncio N, Moreira C, Carvalho L, Lopes JAP. Aggregated dynamic model of active distribution networks for large voltage disturbances. Electr Power Syst Res 2020;178. http://dx.doi.org/10.1016/j.epsr.2019.106006.
[9] Chaspierre G, Denis G, Panciatici P, Cutsem TV. A dynamic equivalent of active distribution network: Derivation, update, validation and use cases. IEEE Open Access J Power Energy 2021;8:497–509. http://dx.doi.org/10.1109/oajpe.2021.3102499.
[10] Bömer JC. On stability of sustainable power systems - network fault response of transmission systems with very high penetration of distributed generation [Ph.D. thesis], Technische Universiteit Delft; 2016, http://dx.doi.org/10.4233/uuid:78bffb19-01ed-48f9-baf6-ffb395be68a0.
[11] Valois-Rodriguez MF, Ungerland J. Evaluation of grid reduction techniques for distribution networks with a high penetration of inverter-based generation. In: IEEE PES innovative smart grid technologies Europe. 2020, p. 824–8. http://dx.doi.org/10.1109/ISGT-Europe47291.2020.9248966.
[12] Load representation for dynamic performance analysis (of power systems). IEEE Trans Power Syst 1993;8(2):472–82. http://dx.doi.org/10.1109/59.260837.
[13] Milanovic J, Matevosyan J, Gaikwad A, Borghetti A, Djokić S, Dong Z, Halley A, Korunović L, Villanueva S, Ma J, Pourbeik P, Resende F, Sterpu S, Villella F, Yamashita K, Auer O, Karoui K, Kosterev D, Leung S, Mtolo D, Zali S, Collin A, Xu Y. CIGRE WG C4.605: Modelling and aggregation of loads in flexible power networks. Tech. rep., CIGRE; 2014.
[14] Joint Working Group C4/C635/CIRED. Modelling of inverter-based generation for power system dynamic studies. Tech. rep., CIGRE; 2018.
[15] Lammert G, Yamashita K, Ospina LDP, Renner H, Villanueva SM, Pourbeik P, Ciausiu F-E, Braun M. International industry practice on modelling and dynamic performance of inverter based generation in power system studies. CIGRE Sci Eng J 2017;8:25–37.
[16] Kundur P. Power system stability and control. New York: McGraw-Hill; 1994.
[17] Ungerland J, Pant P. Challenges of modelling equivalent active distribution grids under consideration of grid forming inverters. In: Virtual 19th wind integration workshop. 2020.
[18] Ungerland J, Lens H. Evaluation of equivalent dynamic active distribution network models with individual and aggregated consideration of grid forming converters. Energy Technol 2023;11. http://dx.doi.org/10.1002/ente.202300336.
[19] Ierna R, Zhu J, Urdal H, Roscoe AJ, Yu M, Dyśko A, Booth CD. Effects of VSM convertor control on penetration limits of non-synchronous generation in the GB power system. In: 2016 15th wind integration workshop, at Vienna. 2016.
[20] ENTSO-E. High penetration of power electronic interfaced power sources. Tech. rep., ENTSO-E; 2017.
[21] Chawda GS, Shaik AG. Power quality mitigation in weak AC grid with low X/R ratios using distribution static compensator controlled by LMF algorithm. In: 2020 IEEE region 10 symposium. 2020, http://dx.doi.org/10.1109/TENSYMP50017.2020.9230727.
[22] CIGRE. Technical brochure WG B4.62: connection of wind farms to weak AC networks (671). CIGRE; 2016.
[23] Brittain JE. Thévenin's theorem. IEEE Spectr 1990;27:42. http://dx.doi.org/10.1109/6.48845.
[24] WECC Renewable Energy Modeling Task Force. WECC PV Power plant dynamic modeling guide. Tech. rep., Western Electricity Coordinating Council (WECC); 2014.
[25] North American Electric Reliability Corporation (NERC). Reliability guideline - parameterization of the DER_A model. Tech. rep., Atlanta, US: NERC; 2019.
[26] DIgSILENT GmbH. PowerFactory 2024 - Technical reference - digsilent grid-forming converter templates. Tech. rep., Gomaringen, Germany: DIgSILENT GmbH; 2024.
[27] WECC. WECC Dynamic composite load model (CMPLDW) specifications. Tech. rep., WECC; 2015.
[28] Strunz K, Abbasi E, Abbey C, Andrieu C, Campbell RC, Fletcher R. Benchmark systems for network integration of renewable and distributed energy resources. Tech. rep., 273, CIGRE; 2014.
[29] Amme J, Pleßmann G, Bühler J, Hülk L, Kötter E, Schwaegerl P. The eGo grid model: An open-source and open-data based synthetic medium-voltage grid model for distribution power supply systems. J Phys: Conf Ser 2018;977. http://dx.doi.org/10.1088/1742-6596/977/1/012007.
[30] Ungerland J. Equivalent dynamic models of active distribution networks with grid following and grid forming converters [Ph.D. thesis], Universität Stuttgart; 2023, http://dx.doi.org/10.18419/opus-13567.
[31] Fördergesellschaft Windenergie und andere Dezentrale Energien. Technical guidelines for power generating units and systems: part 4. Tech. rep., Berlin: FGW e.V.; 2019.
[32] Badrzadeh B, Davis M, Goyal S, Grogan S, Lu J, Villella F, Mahsredjian J, Muthumuni D, Fernandez F, Kuri A, Dall L, Saad H, Escudero M, Schmall J. CIGRE WG C4.56: Electromagnetic transient simulation models for large-scale system impact studies in power systems having a high penetration of inverter-connected generation. Tech. rep., CIGRE; 2022.